Mimicking the Helix with a porous disc for wind tunnel testing

De Vos, Brian; Harder, Bjorn M.; Huisman, Thomas A.; Gutknecht, Jonas; Van Wingerden, Jan Willem

DOI
10.1088/1742-6596/2767/9/092063

Publication date
2024

Document Version
Final published version

Published in
Journal of Physics: Conference Series

Mimicking the Helix with a porous disc for wind tunnel testing

Journal of Physics: Conference Series **2767** (2024) 092063 doi:10.1088/1742-6596/2767/9/092063

Mimicking the Helix with a porous disc for wind tunnel testing

Brian de Vos[1,*], Bjorn M. Harder[1,*], Thomas A. Huisman[1], Jonas Gutknecht[1] and Jan-Willem van Wingerden[1]

[1] Delft University of Technology, Delft Center for Systems and Control, Mekelweg 2, 2628 CD Delft, The Netherlands

[*]These authors have contributed equally

E-mail: B.deVos-3, B.M.Harder@student.tudelft.nl, J.Gutknecht, J.W.vanWingerden@tudelft.nl

Abstract. A promising method to reduce wake effects in offshore wind farms is the Helix approach, which increases the mixing of the wake with the surrounding flow by exciting the individual blade pitch. This increases the wind speed in the wake, resulting in a higher power output at a downstream turbine. Wind tunnel testing is crucial to gather further understanding of the governing mechanisms behind the Helix and its efficiency in larger wind farm arrays. However, model turbines are expensive and complex. Porous Discs (PD) have proven to supply a less expensive and less complex alternative for wake-focused wind tunnel studies. In this study we present a novel PD model to mimic the Helix. The fundamental idea is to mimic the non-uniform, unsteady energy extraction over the rotor plane as observed at a Helix-controlled turbine. For this purpose, we derive a non-uniform porosity distribution over the PD, based on Large Eddy Simulations of a three-bladed turbine controlled with the Helix approach, and the actuator disc theory. The resulting non-uniform PD rotates at the excitation frequency described by the Strouhal number to mimic the Helix. We verified the novel experimental setup with smoke visualisation techniques and thrust measurements at a second PD in the wake and observed the typical characteristics of the Helix wake of a model turbine: First, the wake was deformed into a helical shape, and second, the wake velocity increased depending on the excitation Strouhal number.

1. Introduction

With the increasing demand for renewable energy, offshore wind energy has gained popularity in the past decade [7]. Here, wind turbines can be placed together in so-called wind farms to exploit several advantages, including shared infrastructure and reduced maintenance costs. Despite these advantages, wind farms also give rise to new problems like the wake effect. The wake is a region of less energetic and more turbulent flow caused by the energy extraction of the upstream turbine. A turbine operating at 3 rotor diameters ($3D$) downstream in the wake of an upstream turbine consequently produces up to $\approx 46\,\%$ [1] less power than in the stand-alone case, which negatively impacts the total power output of the wind farm.

Several methods have been presented to mitigate this effect. For example, by yawing the upstream turbine, the wake can be steered away from the downstream turbine. This method was found to increase overall power production using the *FLOw Redirection and Induction in Steady State* tool (FLORIS) [5].

Alternatively, the power production can be increased by enhancing the mixing of the low energetic wake with the high energetic surrounding flow. A first control strategy for enhancing mixing, called Dynamic Induction Control (DIC), was presented by Munters and Meyers [11]. With DIC, the induction factor of an upstream wind turbine is varied sinusoidally over time by changing the collective pitch angle of the rotor. The resulting oscillating thrust force generates vortex-ring-like structures in the wake, which were found to accelerate the breakdown of the wake. Simulations by Munters and Meyers [10] as well as Frederik et al. [4] imply an increased total power output of two aligned turbines as a result of DIC.
However, DIC increases fatigue loads significantly due to cyclical loading on wind turbine components caused by fluctuations in thrust force. Another wake mixing enhancing control strategy was presented by Frederik et al.[3] called the *Helix approach*. It uses Dynamic Individual Pitch Control (DIPC) such that the thrust vector moves off-centre. The blades are continuously pitched with a phase offset, in order to circulate the force vector around the rotor centre, either in a counterclockwise (CCW) or clockwise (CW) circular direction. This generates a helical structure in the wake behind the turbine, which is characterised by a faster wake recovery than in the baseline case. Additionally, this is obtained with a lower cyclical loading than in DIC. A CCW Helix improves the power production more than a CW Helix according to simulations by Frederik et al.[3] and wind tunnel experiments performed by van der Hoek et al. [13]. Frederik et al.[3] observed an increase in total power output of two $5D$ spaced turbines of 7.5% in the CCW case.
A governing parameter for the efficiency of the Helix is the excitation frequency, which is usually characterised by the Strouhal number (St):

$$St = \frac{f_e D}{u_\infty}, \tag{1}$$

Where u_∞ in m/s represents the free-stream velocity, f_e in Hz the excitation frequency and D the diameter in m. Frederik et al.[3] found an optimal Strouhal number between $St = 0.2$ and $St = 0.35$ in terms of velocity increase of the wake at the second turbine.
While conventional wind tunnel testing with scaled-down model turbines provides a satisfactory solution for replicating IPC turbines in wind tunnels, the turbines are expensive and complex, requiring a swash plate assembly to move the individual turbine blades[13]. Therefore, these models are not suitable for testing the impact of the Helix in large-scale wind farms. An alternative to scaled-down model turbines are Porous Discs (PD), which have been found to approximate the far-wake of a conventionally controlled wind turbine in a wind tunnel [6, 14, 2]. Furthermore, Howland et al.[6] have shown that even the steered wake of a yaw-misaligned turbine can be modelled using a PD. The main advantage of using a PD is its reduced complexity compared to a model wind turbine because it eliminates the need for aerofoils, control- and actuation systems, and drive train. These factors reduce the costs of running tests and make testing large scale wind farms more feasible.
In this study, we propose a novel PD model which mimics the Helix in wind tunnel experiments. Based on LES data, we create a non-uniform porosity distribution, which replicates the non-uniform deceleration of the flow over the rotor plane. Rotating the PD results in a helically-shaped wake comparable to the wake of a wind turbine controlled with the Helix.
We validate the Helix PD model with smoke visualisations and thrust measurements at a downstream PD to visualise the shape of the wake and confirm an increase in wind speed at the second turbine respectively. Thus, the reduced complexity of the proposed Helix PD model opens the door to investigate the effect of the Helix in larger wind farms experimentally. Additionally, we gain valuable insights into the governing mechanisms of the Helix, based on the missing phenomena not modelled by the PD. The main contribution of this paper is fourfold: Firstly, we propose a novel experimental setup using PDs to perform Helix experiments. Secondly, we give

the first proof-of-principle of the method using smoke-visualisation and thrust measurements. Thirdly, we conclude the major generation mechanism of the Helix is the non-uniform, unsteady thrust distribution. Lastly, our observations imply an interaction of the inherent wake rotation causes the difference between CW and CCW.
The remainder of the paper is structured as follows: Section 2 describes the methodology used to design the PD. Section 3 focuses on the test-setup and measurement equipment used during the experiment. Lastly, the results are discussed in section 4.

2. Methodology

This section discusses the underlying theory for designing the PD geometry. Firstly, the porosity is related to the local velocity at the turbine rotor. Secondly, we will describe the procedures for generating the porous disc model.

2.1. Relation between velocity deceleration and porosity

In contrast to a greedy controlled wind turbine, the Helix approach leads to a non-uniform, unsteady velocity distribution at $0.03D$ behind the rotor, as shown in Fig. 1. The depicted snapshot of a plane close to the rotor is obtained from a Large Eddy Simulation (LES) of a DTU10MW reference turbine from Frederik et al. [3]. This velocity field rotates around the hub axis at the excitation frequency of the Helix which consequently triggers the Helix.

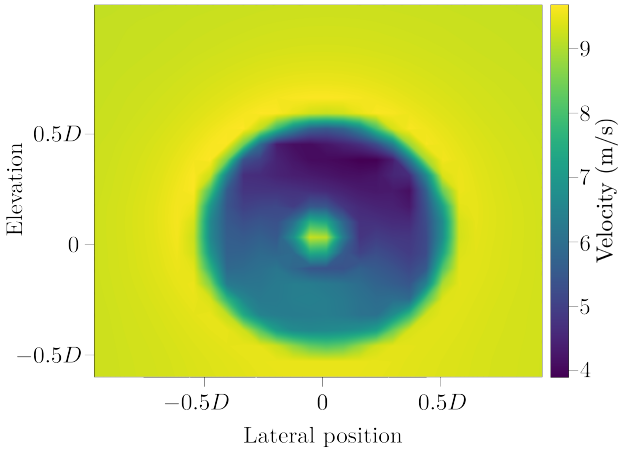

Figure 1: The instantaneous velocity field at $0.03D$ behind the rotor of a turbine controlled with the Helix approach [3].

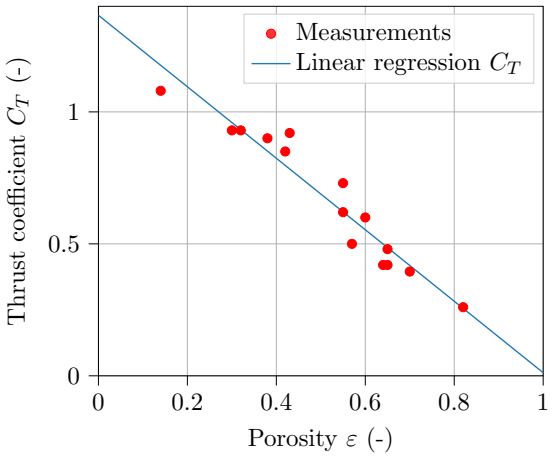

Figure 2: Least squares fit of thrust coefficient C_T and porosity ε to the scattered data points obtained by Lignarolo et al. [9]

We aim to recreate the aforementioned non-uniform velocity distribution with a non-uniform porosity distribution over the PD surface. Rotating the PD with a motor, generates the same unsteady non-uniform velocity field, as observed at a conventional Helix-controlled turbine.
The design of the PD requires a relation between porosity and velocity deceleration. First, we use the actuator disc theory (i.e. momentum theory) to obtain a relation between wind speed at the rotor disc u_1, the free stream velocity u_∞, both in m/s, and axial induction a:

$$u_1 = (1 - a) \cdot u_\infty \tag{2}$$

The dimensionless induction factor a indicates the deceleration of the flow by the rotor. The thrust coefficient C_T can be calculated as follows:

$$C_T = 4a \cdot (1 - a) = 4\left(1 - \frac{u_1}{u_\infty}\right) \cdot \frac{u_1}{u_\infty}. \tag{3}$$

By reviewing multiple PD experiments, Lignarolo et al.[9] derived a relation between the thrust coefficient C_T and the porosity ε. Using the least squares method for linear regression the following expression is obtained from the data shown in Figure 2:

$$C_T = -1.35\varepsilon + 1.37 \tag{4}$$

Finally, equating Equations 3 and 4 leads to the following relation between the velocity distribution and porosity

$$\varepsilon = -2.96\left(1 - \frac{u_1}{u_\infty}\right) \cdot \frac{u_1}{u_\infty} + 1.01, \tag{5}$$

which can then be used to design the PD model.

Figure 1 indicates the rotor decelerates the air more at one side compared to the other side. Additionally, Figure 1 shows a smooth transition in deceleration from one side to the other. This in terms can be simplified by a linear gradient from the minimum velocity $u_{min,wake}$ to maximum velocity $u_{max,wake}$ at opposing sides of the disc through its centre. While $u_{min,wake}$ is obtainable from the simulation data, $u_{max,wake}$ is not. In order to be representative of a real world scenario, the turbine in the simulation is assumed to be operating in the Betz' limit with a resulting induction factor of $a = \frac{1}{3}$. Therefore, the PD needs to have the same mean induction factor $a_{mean} = \frac{1}{3}$. Consequently, $u_{max,wake}$ can be calculated in order to satisfy this condition. Based on these considerations, Equation 5 yields a minimum porosity of $\varepsilon_{min} = 0.298$ and maximum porosity of $\varepsilon_{max} = 0.625$. We locate these values on opposing sides of the disc to then interpolate the intermediate values linearly. This leads to a non-uniform PD (Helix PD) with a mean porosity of $\varepsilon_{mean} = 0.46$. Additionally, we design a baseline PD to simulate a conventionally greedily controlled turbine with the same ε_{mean}. This assures both PDs on their spatial average decelerate the flow similarly to allow for fair comparison of the wake recoveries.

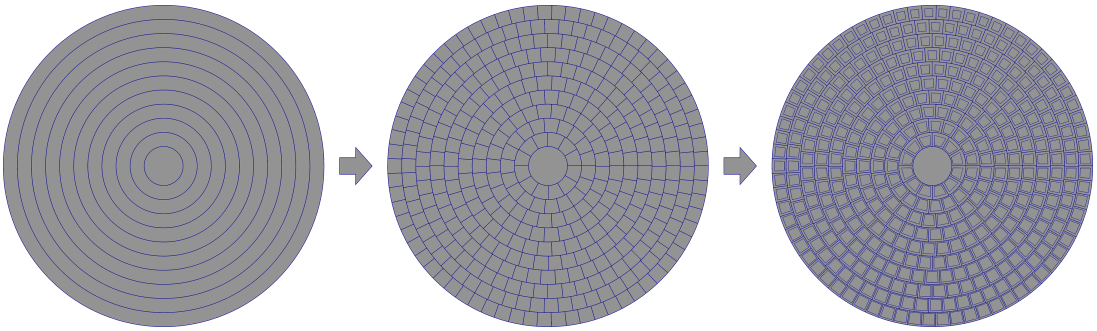

Figure 3: Schematic representation of the three steps to obtain the Helix PD geometry.

2.2. Procedural design of the porous disc

Equation 5 enables us to convert the continuous velocity field to a continuous porosity distribution, which needs to be discretised for creating the PD model. This is done using a procedural meshing approach. Firstly, a disc is divided into equally spaced rings (Figure 3 step 1). Secondly, each ring is divided into segments with the same surface area, as shown in step 2 of Figure 3. Lastly, an inset is created inside each segment which leads to the disc's final porosity as shown in step 3 of Figure 3. The inset width is iterated to fulfil the required porosity at the respective location.

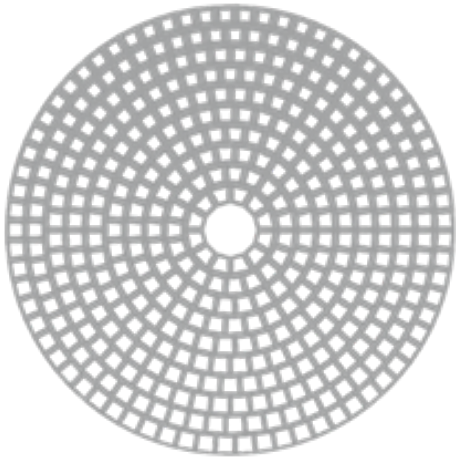

Figure 4: The non-uniform (Helix) porous disc with the lowest porosity at the top and highest at the bottom.

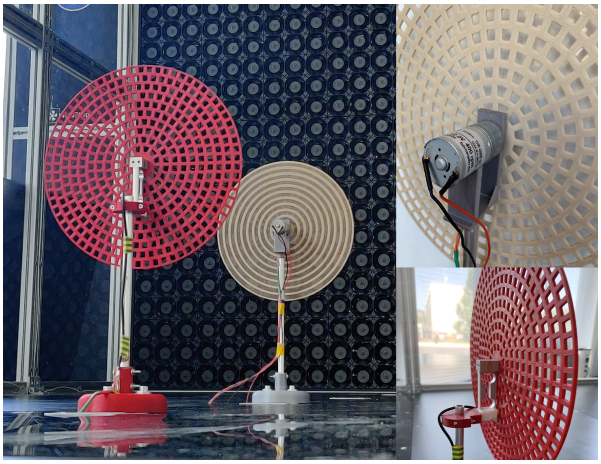

Figure 5: The test set-up as used in the *Windshaper* with the Helix porous disc (white) mounted at $5D$ upstream of the sensor porous disc (red). The top right image shows the DC motor used in the experiment. The bottom right image shows the load-cell and its mounting hardware.

3. Test-setup

This section gives an overview of the experimental setup. Firstly, the specifications of the test model and the wind tunnel equipment are presented. Secondly, we present the smoke visualisation setup, followed, by a description of the thrust measurement setup. Lastly, we will discuss the test plan.

3.1. Test model and testing environment

We use a 3D-printed disc with a diameter of $D_{disc} = 250\,\text{mm}$, similar to the one shown in Figure 4. The rotational frequency of the PD corresponds to the excitation Strouhal number of the Helix. To guarantee a constant, repeatable, rotational frequency the PD is rotated using a PID-controlled DC motor. This results in an error of up to $\epsilon = 0.08\,\text{Hz}$ at the highest rotational frequency of 6 Hz, which is sufficiently accurate for our measurements. Each test model is mounted on an aluminium tower with a height of $h_{tower} = 350\,\text{mm}$ and a diameter of $D_{tower} = 10\,\text{mm}$. The base is a 3D-printed mount which is attached to the wind tunnel floor.
All tests are performed in a *WindShaper* unit at the WindAI Lab at the Delft Center for Systems and Control (DCSC), a wind tunnel containing an array of 729 individually controllable fan modules. In our experiments, the *WindShaper* provides an outflow of $u_{\text{inf}} = 5\,\text{m/s}$ according to the calibration sheet. The PDs are placed in a closed test section with a cross sectional area of $4.84\,\text{m}^2$. Furthermore, the blockage ratio for this experiment is 1.0 % Lastly, the turbulence level has not yet been validated or quantified for the *WindShaper*.
A smoke dispenser, mounted upstream of the PD, allows us to observe the shape and temporal development of the wake behind the PD. Each experiment is filmed using a *Full HD*, 240 frames per second and a *4K Ultra HD*, 60 frames per second camera.

3.2. Thrust measurement

Whilst smoke provides a picture of the wake shape, it does not allow for a quantitative validation of the wake recovery. Therefore, we mount a second PD model, equipped with a

load cell at the hub, in the wake of the Helix PD. This sensor turbine allows us to measure the thrust force at the respective downstream position in the wake of the Helix PD ($F_{T,Helix}$) and baseline PD ($F_{T,baseline}$). Since the PDs are designed to have the same thrust coefficient, $C_{T,Helix} = C_{T,baseline}$, the ratio between $F_{T,Helix}$ and $F_{T,baseline}$ scales with the square of the disc-averaged velocity:

$$\frac{F_{T,Helix}}{F_{T,baseline}} = \frac{\frac{1}{2}C_{T,Helix}\rho A{u^2}_{Helix}}{\frac{1}{2}C_{T,baseline}\rho A{u^2}_{baseline}} = \frac{{u^2}_{Helix}}{{u^2}_{baseline}} \tag{6}$$

Thus, the thrust measurements allow for a quantitative comparison of the wake recovery between the different wakes. The sensor PD, is a baseline PD which means the thrust measurement would be comparable to using a greedy controlled turbine downstream of the Helix. The load-cell is manufactured by *Mavin* and has a relative output error of 0.03 %. Lastly, the amplifier is an off the shelf *HX711* analog-to-digital converter amplifier board.

3.3. Test plan and general experiment setup

We evaluate the Helix PD at the Strouhal numbers $St = 0.10, 0.15, 0.20, 0.25$, and 0.30 for both a CCW and CW rotating PD. The baseline PD is tested with and without rotation. Firstly, a stationary test provides a baseline thrust value with which we can normalise the thrust increase caused by the Helix PD. Secondly, a test at 5 Hz rotational speed ($St = 0.25$) is done to check the influence of a rotating PD on the wake in general and ensure the difference seen in the thrust measurements is a direct result of the non uniform porosity distribution, not the inherent rotation. The sensor PD is placed at a downstream position of $5D$, equivalent to the turbine spacing used in previous studies [3, 8, 12, 13].

4. Results

Prior to the model validation, we validate the design objective of equal thrust coefficients for the Helix PD and the baseline PD. For this purpose, the thrust of both PDs in stationary and rotating states is measured with strain gauges at the tower. They are found to deviate by 6 %, which is in a suitable range for the following measurements.

The remainder of this section presents the experimental results. Firstly, the visual validation using smoke is discussed. Secondly, we compare the wake recovery of different settings quantitatively based on the thrust measurements at the sensor PD.

4.1. Smoke visualisation of the PD wake

Figure 6 shows the top view of a smoke visualisation of the Helix PD wake (top row) and the baseline PD wake (bottom row) as seen during a single rotation period of the PD at the Helix excitation frequency f_e corresponding to a Strouhal number of $St = 0.20$. The differences are significant: the Helix wake shows horizontal deflections first to the right and then to the left. Whereas, the baseline wake is symmetric around the centre line. This indicates the Helix PD induces wake dynamics not present in the baseline case. The video footage, which can be accessed via the QR code, reveals a clearer impression of the dynamics of both wakes. The wake of the baseline PD is axisymmetric and quasi-steady, whereas the Helix PD generates a helical shape that rotates at the same speed as the PD. Thus, the smoke visualisation indicates the PD model successfully generates a helical shape in the wake.

4.2. Wake recovery quantified with thrust measurements

Figure 7 presents the resulting thrust averaged over $\Delta t = 120$ s at different Strouhal numbers. The CCW Helix is represented in blue and the CW Helix is shown in orange.

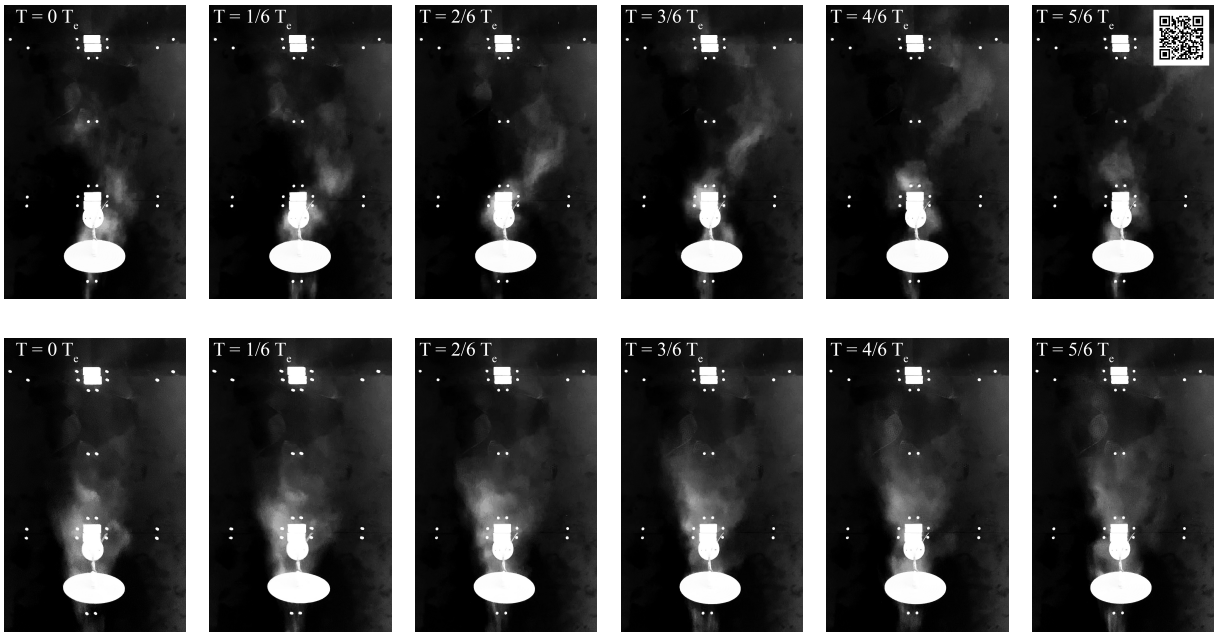

Figure 6: Top view snapshots of the PD wakes visualised with smoke behind the Helix PD (top row) and rotating baseline PD (bottom row) progressing over a single rotation with excitation frequency f_e and excitation period $T_e = 1/f_e$. The respective f_e corresponds to a Strouhal number of $St = 0.20$. The QR code links to the video footage of the experiments.

All measurements are normalised w.r.t. to the baseline case $F_{T,Baseline}$. The sensor PD is placed $5D$ downstream of a baseline PD.
An increased thrust, which implies an increased wake recovery, at $5D$ is observed for all the researched Strouhal numbers. Figure 7 indicates a strong dependence of the wake recovery on the Strouhal number with an optimum at $St = 0.2$. At the peak, the PD turbine has a thrust increase of 67 % and 69 % for CW and CCW, respectively. According to Equation 6, this implies a velocity increase at $5D$ of 29% and 30% for CW and CCW, respectively. Thus, the Helix PD exhibits the major characteristics of the Helix observed in previous studies [3, 12, 13]. These characteristics are generated without modelling the blades and consequently the tip vortices. Therefore, it can be concluded, that the major generation mechanism of the Helix is related to the non-uniform, unsteady thrust distribution. Effects related to the tip vortices, like accelerated vortex pairing, can be excluded as a major effect behind the Helix.
As is evident from Figure 7, the wake recovery of the CW and CCW Helix are equal within the confidence intervals. At a glance, this contradicts previous studies where significant differences between the CW and CCW Helix have been observed [3, 13]. However, this observation can be explained by the phenomena captured by the PD model and those not captured. In contrast to the PD wake, a real turbine wake shows a circulation and a hub vortex, which both rotate against the direction of rotation of the rotor. The direction of rotation does not change with the CW or CCW Helix. As the PD does not model the blades, its wake lacks this inherent wake rotation. Consequently, the CW and CCW wakes of the PD are symmetric, thus, the equal wake recovery of the CW and CCW Helix are to be expected. This observation implies the difference between the CW and CCW Helix at a real turbine is due to an interaction with the inherent wake rotation.

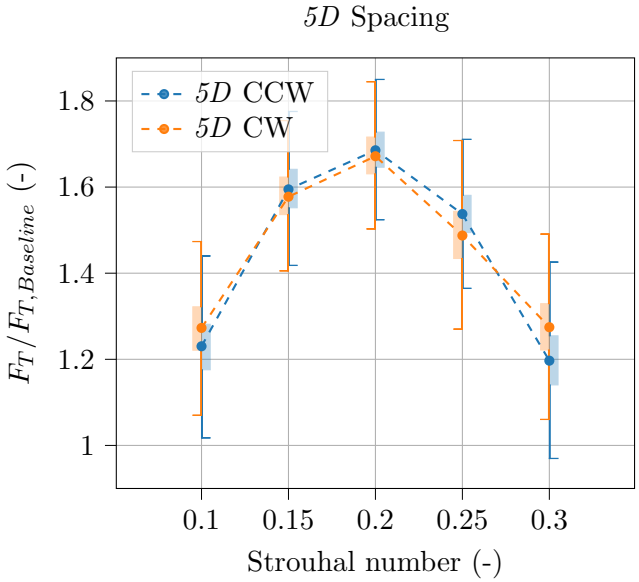

Figure 7: Thrust output of the downstream turbine for $5D$ spacing measured in a range of different Strouhal numbers. Each point represents the thrust averaged over 120s and normalised w.r.t the baseline.

5. Conclusions

We propose a novel experimental setup for modelling the Helix wake using a rotating Porous Disc (PD) with a non-uniform porosity. This is intended to replicate the wind speed deceleration of a real Helix-controlled turbine. Using smoke visualisation, we show the wake takes a helical shape. Its effect on the wake recovery is quantified by measuring the thrust at a downstream PD, which increases with wind speed. The observed increase of the wake recovery follows a dependency on the Strouhal number as observed in previous studies. Consequently, the presented Helix PD model captures major characteristics of the Helix of a real turbine and thereby flattens the path towards studying the efficiency of the Helix in larger wind turbine arrays experimentally. Since the PD model is a simplification of a wind turbine, some effects such as hub and tip vortices are not present. Nonetheless, in all scenarios the Helix PD shows an increase of thrust at the sensor PD. Therefore, it can be concluded the overall effect of the Helix is not necessarily governed, but merely influenced by the phenomena not modelled in our PD model.
In contrast to previous studies, no significant differences in the efficiencies of a CCW and CW Helix were observed. Consequently, we conclude the difference between the CW and CCW Helix is due to phenomena not captured in our model like the hub vortex and/or the inherent wake rotation. Further research may focus on validating our results with Particle Image Velocimetry (PIV) and then applying the model with multiple PDs to evaluate the effect of the Helix in a larger turbine array.

6. Acknowledgements

This work is part of Hollandse Kust Noord wind farm innovation program where CrossWind C.V., Shell, Grow, Eneco and Siemens Gamesa are teaming up; funding for the PhDs was provided by CrossWind C.V. and Siemens Gamesa. We want to express our gratitude to W.H.A. Wien and R.J.M. Willekes whom without, this research would not have been possible.

References

[1] Muyiwa S. Adaramola and Per Å. Krogstad. Experimental investigation of wake effects on wind turbine performance. *Renewable Energy*, 36(8):2078–2086, 2011.

[2] Sandrine Aubrun, Stéphane Loyer, Philip E. Hancock, and Paul Hayden. Wind turbine wake properties: Comparison between a non-rotating simplified wind turbine model and a rotating model. *Journal of Wind Engineering and Industrial Aerodynamics*, 120:1–8, 2013.

[3] Joeri A. Frederik, Bart M. Doekemeijer, Sebastiaan P. Mulders, and Jan-Willem van Wingerden. The helix approach: Using dynamic individual pitch control to enhance wake mixing in wind farms. *Wind Energy*, 23(8):1739–1751, 2020.

[4] Joeri A. Frederik, Robin Weber, Stefano Cacciola, Filippo Campagnolo, Alessandro Croce, Carlo Bottasso, and Jan-Willem van Wingerden. Periodic dynamic induction control of wind farms: proving the potential in simulations and wind tunnel experiments. *Wind Energy Science*, 5(1):245–257, 2020.

[5] P. M. O. Gebraad, F. W. Teeuwisse, J. W. van Wingerden, P. A. Fleming, S. D. Ruben, J. R. Marden, and L. Y. Pao. Wind plant power optimization through yaw control using a parametric model for wake effects—a cfd simulation study. *Wind Energy*, 19(1):95–114, 2016.

[6] Michael F. Howland, Juliaan Bossuyt, Luis A. Martínez-Tossas, Johan Meyers, and Charles Meneveau. Wake structure in actuator disk models of wind turbines in yaw under uniform inflow conditions. *Journal of Renewable and Sustainable Energy*, 8(4):043301, Jan 2016.

[7] International Energy Agency (IEA). Offshore wind outlook 2019, 2019. License: CC BY 4.0.

[8] Henry Korb, Henrik Asmuth, and Stefan Ivanell. The characteristics of helically deflected wind turbine wakes. *Journal of Fluid Mechanics*, 965:A2, 2023.

[9] Lorenzo E. M. Lignarolo, Daniele Ragni, Carlos J. Ferreira, and Gerard J. W. van Bussel. Experimental comparison of a wind-turbine and of an actuator-disc near wake. *Journal of Renewable and Sustainable Energy*, 8(2), 03 2016. 023301.

[10] Johan Meyers, Carlo Bottasso, Katherine Dykes, Paul Fleming, Pieter Gebraad, Gregor Giebel, Tuhfe Gocmen, and J.W. van Wingerden. Wind farm flow control: prospects and challenges. *Wind Energy Science*, 7(6):2271–2306, 2022.

[11] Wim Munters and Johan Meyers. Effect of wind turbine response time on optimal dynamic induction control of wind farms. *Journal of Physics: Conference Series*, 753(5):052007, sep 2016.

[12] Emanuel Taschner, Aemilius A.W. van Vondelen, Remco A. Verzijlbergh, and Jan-Willem van Wingerden. On the performance of the helix wind farm control approach in the conventionally neutral atmospheric boundary layer. *Journal of Physics: Conference Series*, 2505(1):012006, may 2023.

[13] Daan van der Hoek, Bert Van den Abbeele, Carlos S. Ferreira, and Jan-Willem van Wingerden. Maximizing wind farm power output with the helix approach – experimental validation and wake analysis using tomographic PIV, 2023.

[14] Magnus K. Vinnes, Stefano Gambuzza, Bharathram Ganapathisubramani, and R. Jason Hearst. The far wake of porous disks and a model wind turbine: Similarities and differences assessed by hot-wire anemometry. *Journal of Renewable and Sustainable Energy*, 14(2):023304, 2022.